AAS 26-697

LUNAR SUNRISE ORBITS AND APPLICATIONS TO NASA CLPS MISSIONS

Anthony L. Genova*, Dylan Morrison-Fogel†, Ryan P. Russell‡, Carter J. Van Hammond§, & Regina Blue§§

NASA's Commercial Lunar Payload Services (CLPS) initiative has stimulated the lunar economy with recent and planned landings on the Moon by U.S. companies. The primary purpose of this paper is to define, discover, and analyze Lunar Sunrise Orbits (LSOs), sun-synchronous and near repeat ground orbits at the Moon that are phased for a spacecraft to encounter a landing site at sunrise. This unique class of orbits can be used as a nominal staging orbit for future CLPS lunar lander missions to provide backup landing opportunities at lunar sunrise. An LSO reference orbit adds mission resiliency and robustness without any propellant cost in the case of a missed descent maneuver in low lunar orbit. Classical lunar frozen orbits will also be explored in the context of LSOs with applications shown for future CLPS missions and concepts.

INTRODUCTION

NASA's Commercial Lunar Payload Services (CLPS) initiative contracts U.S. companies to provide lunar payload services that advance capabilities for scientific, technological, or commercial development of the Moon [1]. Under CLPS, three lunar landers have already reached the lunar surface at the time of this writing while several more missions are planning to land on the lunar nearside, farside, and south pole region over the next couple of years [2].

Lunar sunrise orbits (LSOs) are defined as orbits with near repeat ground tracks that pass over a specified lunar surface site at successive lunar sunrise times. CLPS landers generally land at (or shortly after) local lunar sunrise to ensure that most of the lunar day can be used for surface operations given the challenges of surviving the cold lunar night. For an arbitrary staging orbit, if a lunar descent is delayed for any reason, the spacecraft will approximately return to the landing site after the moon completes 1 synodic revolution. However, the return geometry defined by the spacecraft, landing site, and terminator is not exact due to inertial rotation of the terminator, and due to perturbations from the Earth and the non-spherical gravity of the Moon. The exact return arrival conditions will not be at sunrise and the second landing maneuver will be substantially different and may be prohibitively more expensive than that of the nominal. Alternatively, if an LSO is chosen as a staging orbit, the return arrival conditions and landing maneuver design will be identical to that of the nominal.

* NASA CLPS Astrodynamics Subject Matter Expert, Spaceflight Div., NASA Ames Research Ctr., Moffett Field, CA
† Spaceflight Dynamicist, Axient, NASA Ames Research Ctr., Spaceflight Division, Moffett Field, CA
‡ Professor, Hayden Head Centennial Professorship, Cockrell School of Eng., The Univ. of Texas at Austin, Austin, TX
§ Masters Student, Cockrell School of Engineering, The University of Texas at Austin, Austin, TX
§§ NASA CLPS Deputy Programmatic Manager, NASA Johnson Space Center, NASA, Houston, TX

By utilizing one or more of these LSOs, mission resiliency can be achieved by ensuring existence of backup landing windows at lunar sunrise in case the descent orbit initiation (DOI) and/or associated maneuvers are missed for any reason (e.g., temporary loss of communication, thruster malfunctions, maneuver execution errors, orbit determination problem, off-nominal attitude profile, landing site problems, etc.).

The primary goal of this paper is to present and analyze several options for different types of LSOs and show applications specifically in the context of NASA CLPS missions. Results are presented from a theoretical perspective utilizing perturbation sources from well understood lower fidelity models, as well as numerical scans using *STK Astrogator* using a high-fidelity force model in the full ephemeris model. LSOs are then applied to CLPS missions with non-polar landing sites on the lunar nearside and farside, with delta-V of correction maneuvers quantified assuming both near-term (backup landing attempts within days of the nominal plan) and longer-term recoveries (i.e., over successive lunar sunrises).

LUNAR SUNRISE ORBITS FOR SHORT-DURATION SURFACE MISSIONS

For short-duration lunar surface missions, landing at local sunrise is highly desirable. A landing that occurs near sunrise maximizes the available surface daylight interval, which is particularly valuable for solar-powered systems and when landers are not designed to survive the lunar night. This consideration is especially relevant for CLPS missions and other short-duration landers, that seek to maximize science and operations within a single lunar day [2].

This operational objective introduces a timing problem. Reaching the correct latitude and longitude is not enough; the local solar time must also be appropriate for landing. The landing must occur when the intended site is on or near the advancing Sun terminator. In other words, the descent opportunity is constrained simultaneously by surface geography and by illumination geometry. Since the Moon rotates slowly, a spacecraft that misses its descent opportunity must wait approximately one synodic month before it approximately returns to the same surface location. However, the lighting conditions at that later opportunity will generally no longer correspond to local sunrise. A one-month wait may recover the ground track geometry, assuming the orbit is designed to have a repeat ground track (RGT). However, the orbit will not automatically recover the illumination geometry. For a mission that requires a sunrise landing, this distinction is critical.

For the landing application, it is useful to distinguish between the broader class of a sun-synchronous orbit (SSO) and the specific LSO subset solution. A SSO is defined here as an orbit whose nodal precession rate is matched to the apparent motion of the Sun, so that the orbit maintains a constant local solar time at a specified node or surface-crossing condition over successive repeat cycles. A LSO is a particular realization of such a solution, obtained when the epoch is selected and the spacecraft is phased along the body-fixed periodic orbit so that the corresponding landing location coincides with local sunrise. In that sense, sun-synchronicity is a property of the orbit family, whereas the sunrise condition is achieved through the specific choice of epoch and phasing within that family.

A useful way to recover both constraints is to place the spacecraft in a long-lifetime repeat ground track (LRGT) SSO [3]. In this context, a LSO implies by definition that the repeat ground track geometry and sun-referenced orientation are coordinated so that repeated passes over a target region occur at or near lunar sunrise. If the spacecraft arrives at the Moon with appropriate phasing, then a LRGT SSO can become a LSO timed such that the vehicle repeatedly passes over the intended landing site near the local sunrise terminator. The use of an LSO nominal staging orbit leads to a built-in contingency option at little to no cost. If the first descent opportunity is missed, the orbiter will return to essentially the same descent region under nearly the same lighting conditions one repeat cycle later.

A companion paper develops the theoretical framework for these solutions and identifies four distinct LSO classes [4]. The work presented here focuses on the application to lunar sunrise landing support. In particular, attention is restricted to the classes that are most relevant to CLPS missions including: 1) low-altitude, near-circular, mid-latitude families, 2) mid-latitude, eccentric, classic frozen families, and 3) high-altitude, near-polar, near-circular, mildly unstable families.

LUNAR REPEAT GROUND TRACK SUN-SYNCHRONOUS ORBIT CLASSES

A LSO is exactly periodic in the Moon body-fixed frame under the following assumptions: 1) the Moon's spin axis is inertially fixed as the body-fixed z axis, and the rotation rate is constant 2) the Earth is static in this body-fixed frame at a constant distance on the x axis. 3) the only accelerations on the spacecraft are due to the Moon's point mass and nonspherical gravity and the Earth's point mass gravity. The described model can be characterized as a Hamiltonian system [3], featuring integrals of motion, equilibria, periodic solutions, stability indices, and other dynamical systems properties arising from Floquet theory. This simplified model does not include the high-accurate ephemeris locations of the Earth, nor other perturbations such as the solar gravity or solar radiation pressure (SRP). However, the simplified model is also not necessarily low-fidelity as it can include an arbitrarily large lunar gravity field and still accounts for the average Earth gravity. This simplified model is useful for identifying and characterizing LSOs [4] among the infinite options of orbits in the vicinity of the Moon. LSOs in this medium-fidelity model will have exactly periodic return conditions for a contingency landing. Interesting solutions in this medium-fidelity Hamiltonian model can be considered in a higher-fidelity model, where the return conditions will be nearly periodic.

The medium fidelity Hamiltonian model is the restricted three-body model superposed with non-spherical gravity model deemed the RTBP+NS model. In this formulation, the averaged third-body effects of the Earth are represented through the RTBP, while the lunar gravitational effect is modeled using the 660b GRAIL gravity field [5]. The spherical harmonic representation of the lunar potential is implemented using the nonsingular Cartesian formulation of Pines [6]. The gravitational potential is written as

$$U(\mathbf{r}) = \frac{\mu}{r}\sum_{n=0}^{\infty}\sum_{m=0}^{n}\left(\frac{R}{r}\right)^{n} A_{nm}\left(\frac{z}{r}\right)\left[C_{nm}R_{m}\left(\frac{x}{r},\frac{y}{r}\right) + S_{nm}I_{m}\left(\frac{x}{r},\frac{y}{r}\right)\right]$$

where

$$R_m(s,t) = \Re\{(s+it)^m\}, \qquad I_m(s,t) = \Im\{(s+it)^m\}$$

and

$$s = \frac{x}{r}, \qquad t = \frac{y}{r}, \qquad p = \frac{z}{r}, \qquad r = \sqrt{x^2+y^2+z^2}$$

Here, μ is the lunar gravitational parameter, R is the reference radius, and $\mathbf{r} = [x\,y\,z]^T$ is the body-fixed position vector (see Fig. 1). The coefficients C_{nm} and S_{nm} are the fully normalized coefficients of the adopted GRAIL gravity model. GRAIL resolved the lunar gravity field to very high degree and order, revealing strong mascon structure that significantly influences low-altitude orbital motion [5]. In this work, the spherical harmonic series is truncated at various levels, depending on the orbit regime.

Solid tides are not modeled explicitly beyond their mean contribution. The J_2 and C_{22} coefficients are modified to account for the mean terms of the dynamical and solid tides according to

$$J_2 = -\bar{C}_{20} = 9.092250523496001 \times 10^{-5}$$
$$\bar{C}_{22} = 3.474597377910000 \times 10^{-5}$$

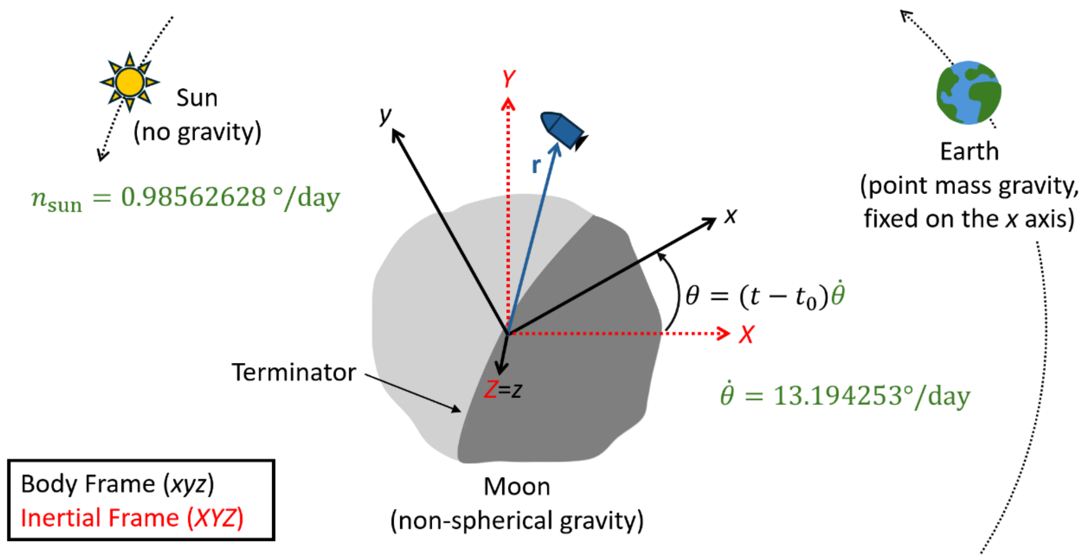

Figure 1. Geometry and notation for the RTBP+NS model

The dynamical tides are otherwise ignored. The model also assumes the lunar spin axis is inertially fixed, ignoring nutation and precession. This Hamiltonian RTBP+NS framework admits a generalized Jacobi constant and stability indices b1 and b2 derived from the monodromy matrix. Linear stability require that the absolute values of b1 and b2 are real and less than or equal to two [7]. This RTBP+NS model, shown in Fig. 1, is well suited for broadly scanning and evaluating the design space while also providing a dynamical basis for more focused high-fidelity grid searches.

The companion paper identifies four primary classes of LRGT SSOs [4]. The first LSO class consists of stable, low-altitude, near-circular solutions with orbital periods close to one lunar day [8]. These orbits are constrained to mid-latitudes, maintain small eccentricity, and provide frequent low-altitude access to the same surface regions. These orbits are heavily perturbed by the nonspherical lunar gravity field, requiring a high-fidelity GRAIL-derived field. The second LSO class consists of stable classic frozen solutions characterized by low perilunes, high apolunes, fixed to remain over either hemisphere [9]. The third LSO class consists of circulating eccentric solutions at higher altitude, with exact repeat times that are much longer, typically on the order of many months to about a year [10]. The fourth LSO class consists of high-altitude, near-circular solutions with orbital periods also around one lunar day. This class of orbits permit high-altitude, high-inclination solutions without requiring extended repeat periods, but exist within a mildly unstable dynamical regime. The mild instability will likely require station-keeping to maintain repeatability. The second, third, and fourth classes are higher altitude orbits governed primarily by the third-body perturbation from the Earth. These orbits can therefore be analyzed using truncated lunar gravity fields.

All four classes are dynamically interesting, but they are not equally useful for the operational problem considered here. If the objective is to recover from a missed landing attempt while preserving near-sunrise illumination at the target site, then the repeat time must be short enough to be useful in a mission operations sense while also providing near-surface perilunes. The first and second LSO classes (low-altitude and classic frozen families, respectively) satisfy this requirement because their repeat behavior occurs on the scale of roughly one lunar month and their minimum altitudes bring them close to the lunar surface. The third LSO class, circulating and eccentric, will have approximately repeating ground tracks every synodic month, but the exact repeat condition is closer to a year. Each month, the return to the landing site would have varying altitudes and descent burn profiles. The lack of monthly repeatability makes this class of LSOs less relevant for the current application. The fourth LSO class of high-altitude orbits is attractive because their inclinations make the polar regions accessible. However, these orbits have high perilunes, making the lunar descent inherently risky with either staged reductions of the perilune or a more expensive and less conventional direct descent maneuver.

While the identified third and fourth LSO classes may be of interest for some applications, the remainder of this paper will focus on the first two LSO classes: the low-altitude and classic frozen classes.

The goal is not to survey the full solution space, but rather to show how representative members of these two families can support the sunrise-landing application. One representative low-altitude LSO and one representative classic frozen LSO are examined in detail. The low-altitude case is taken from the N = 342 family, and the classic frozen case is taken from the N = 27 family, where:

> *N: Integer number of full precessions of the spacecraft orbital plane relative to the Earth-Moon line.* (Approximately the number of revolutions of the apparent Earth around the Moon.)
>
> *M: Integer number of spacecraft revolutions about the Moon*

The two presented examples capture the principal trade between the two most operationally relevant LSO classes. The low-altitude family provides a nearly circular, consistently low lunar orbit, which is attractive for persistent proximity to the landing site and for surface-focused observation or relay geometry. This first class is most similar to a conventional low-altitude staging orbit prior to a lunar descent. The classic frozen LSO class provides greater radial variation and broader viewing geometry, at the cost of having less low-altitude exposure to potential landing sites. Both classes, however, can be designed to satisfy the same basic sunrise-orbit objective: repeated access to a desired landing region when that region lies near the sunrise terminator.

For details on the generation of the LSO families and specific solutions, see Ref. [4]. Note that the periodic LRGT orbits exist as families characterized by M:N, while each LSO is root solved as only a single solution within each family that has matched the precession rate of the terminator. A family of M:N periodic LRGT orbits may or may not include one or more LSO solutions.

REPRESENTATIVE LUNAR SUNRISE ORBIT RESULTS

Two representative LRGT SSO solutions are now considered in detail. The first is the $N = 342$ member of the low-altitude family, and the second is the $N = 27$ member of the classic frozen family.

Low-Altitude Example Orbit: N = 342, M = 1

The $N = 342$ low-altitude family is summarized in Fig. 2. The evolution of orbital elements shows that the semimajor axis remains tightly bounded while eccentricity and (retrograde) inclination undergo modest oscillations. The body-fixed trajectory remains close to the lunar surface over the full repeat cycle, consistent with the intended low-altitude operating concept. The stability indices indicate that the solution is linearly stable, and the bounded motion in the eccentricity plane shows that the eccentricity vector undergoes periodic motion with magnitude varying between 0.0128 and 0.0343.

From the standpoint of the sunrise-landing application, the main value of this solution is its combination of repeatability and surface proximity. Because the orbit remains near-circular and low-altitude, it returns to the same landing region 1 month later with no variation in geometry in this medium fidelity RTBP+NS model. When phased correctly at lunar arrival, this family can support a sunrise descent opportunity with a periodic monthly contingency at any latitude below ~33 degrees given orbit inclination is constrained to greater than ~147 degrees.

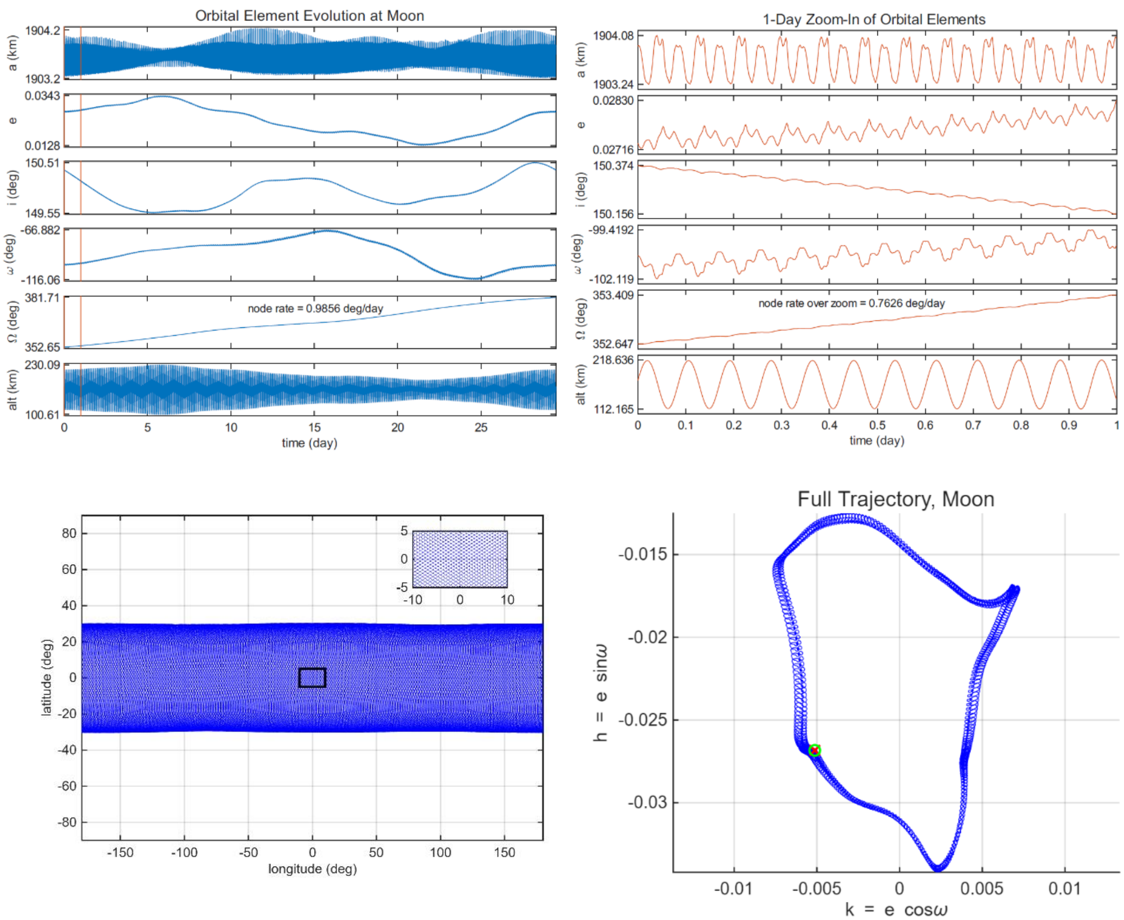

Figure 2: Representative $N = 342$ low-altitude LSO.
b1 = 1.4652120168901004 & b2 = 2.0023837677614287

***Classic Frozen Example Orbit*: *N* = 27, *M* = 1**

The classic frozen LRGT SSO family provides a second operationally relevant way to realize a lunar sunrise orbit. The representative N = 27 orbit is summarized in Fig. 3. In contrast to the low altitude example, the classic frozen solution exhibits a substantially larger radial excursion over each orbit, as expected from its higher eccentricity. The argument of perilune is frozen at +90◦, keeping each perilune at a similar latitude. The orbit reaches a higher range of latitudes compared to the first example, but only a small range of latitudes with low perilune. The associated stability indices indicate that the solution is linearly stable. The trajectory in the eccentricity plane again forms a closed, bounded pattern, with the eccentricity magnitude varying periodically between 0.7382 and 0.7785, consistent with the classic frozen-orbit characteristic showing small librations around a fixed point.

For the sunrise-landing application, this family offers a somewhat different operational trade. The low-altitude family emphasizes continuous proximity to the landing site, whereas the classic frozen family introduces larger altitude variation in exchange for a different viewing and access geometry. A lander staged from such an orbit can still revisit the same site near sunrise after an additional repeat cycle, but the orbit does not remain as uniformly close to the surface as the low-altitude family. Depending on communications geometry, navigation considerations, and desired surface access characteristics, this altitude variation may be considered a drawback, an acceptable trade, or an advantageous geometry.

Most relevant here, the $N = 27$ classic frozen solution still accomplishes the primary sunrise orbit objective. It preserves the coupling between repeat ground track behavior and sun-referenced timing well enough to return the spacecraft to the same general landing site under nearly the same local lighting conditions. Thus, it provides a second viable architecture for descent staging and missed-opportunity recovery.

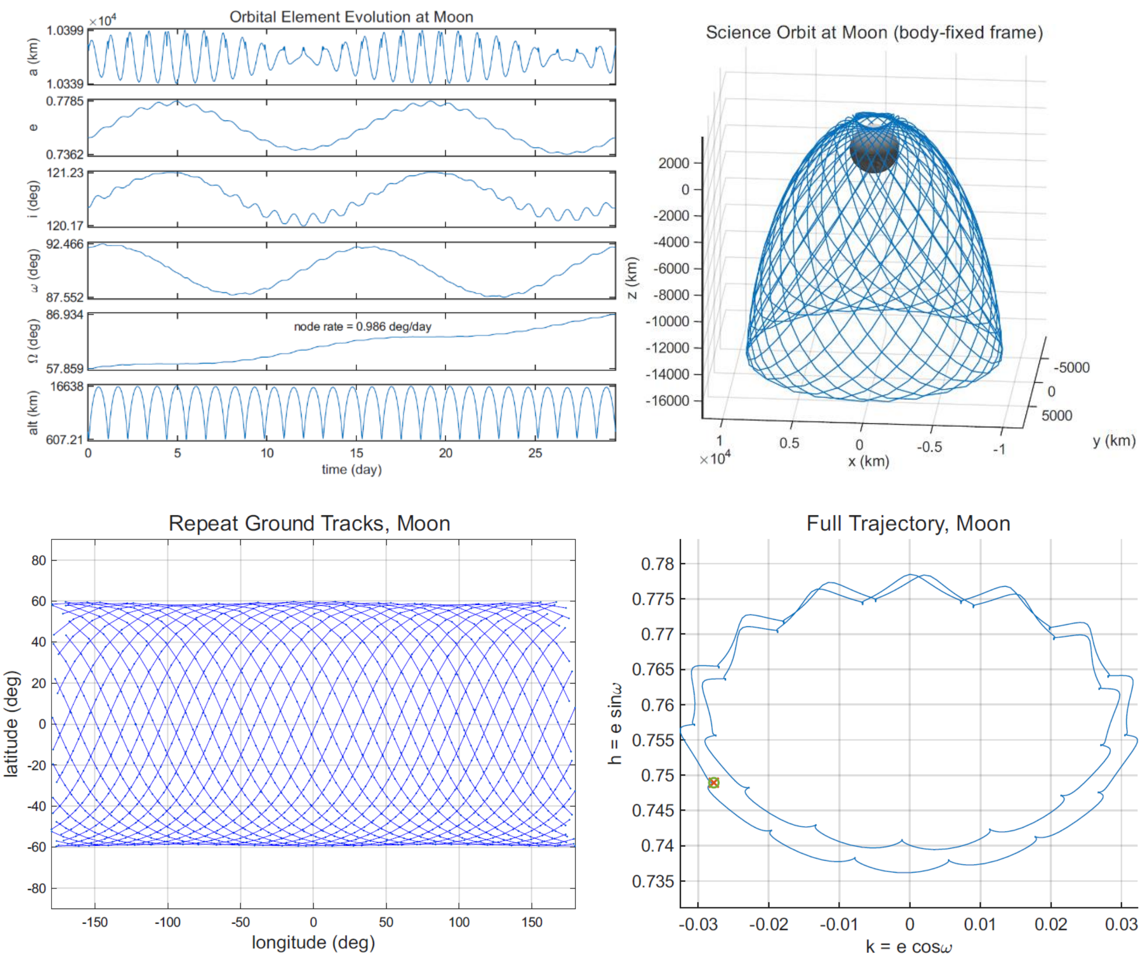

Figure 3: Representative $N = 27$ classic frozen LSO.
b1 = 1.0459519179817418 & b2 = 2.0000052854972177

DISCUSSION

The two representative results illustrate the central contribution of this paper. Lunar sunrise orbits are not simply lunar analogs of terrestrial sun-synchronous orbits, but rather repeat ground track solutions whose sun-referenced timing can be exploited for surface mission resiliency. For CLPS and other short-duration landers, the key benefit is not just illumination-aware orbital motion in the abstract, but the specific ability to preserve both target-site access and sunrise lighting across repeated descent opportunities.

The low-altitude and classic frozen LSO families both support this concept because their repeat times are on the order of one lunar month [7, 8]. This time scale is operationally meaningful for a mission that may need to stand down from one descent attempt and recycle to another. Between the LSO families, the low-altitude solution is especially attractive for its broad reachability to low latitude landing sites, limited altitude variation, and a more surface-focused orbital geometry. The classic frozen solution remains a useful alternative when its larger radial excursion and associated geometry are acceptable or desirable. In either case, the results show that appropriately phased LSOs can act as true LSOs for short duration surface missions.

The two presented baseline orbits are representative classes of a broad search of useful SSO orbits at the Moon [4] and are operationally relevant for CLPS-like landing missions that benefit from one month repeat cycles. They are also long term stable and exactly repeating in the medium fidelity RTBP+NS model. The next section considers these applications in a high-fidelity model that includes ephemeris locations for the Earth and Sun, solar gravity, and SRP.

NUMERICAL HIGH-FIDELITY SEARCH

For the numerical scan to follow, the perilune altitude is set to 100 km given its proximity to the previously studied 95X206 km frozen LLO [11] and since most LLOs and lander missions utilize an altitude of ~100 km. To determine the initial apolune altitude to use in the numerical scan, using the same assumptions and constraints from [11], an apolune scan from 210 to 500 km was performed. It was found that the lowest range in $\text{RAAN}_{\text{Moon-Sun}}$, for most values of initial lunar orbit inclination, was yielded when apolune altitude = 210 km (Fig. 4).

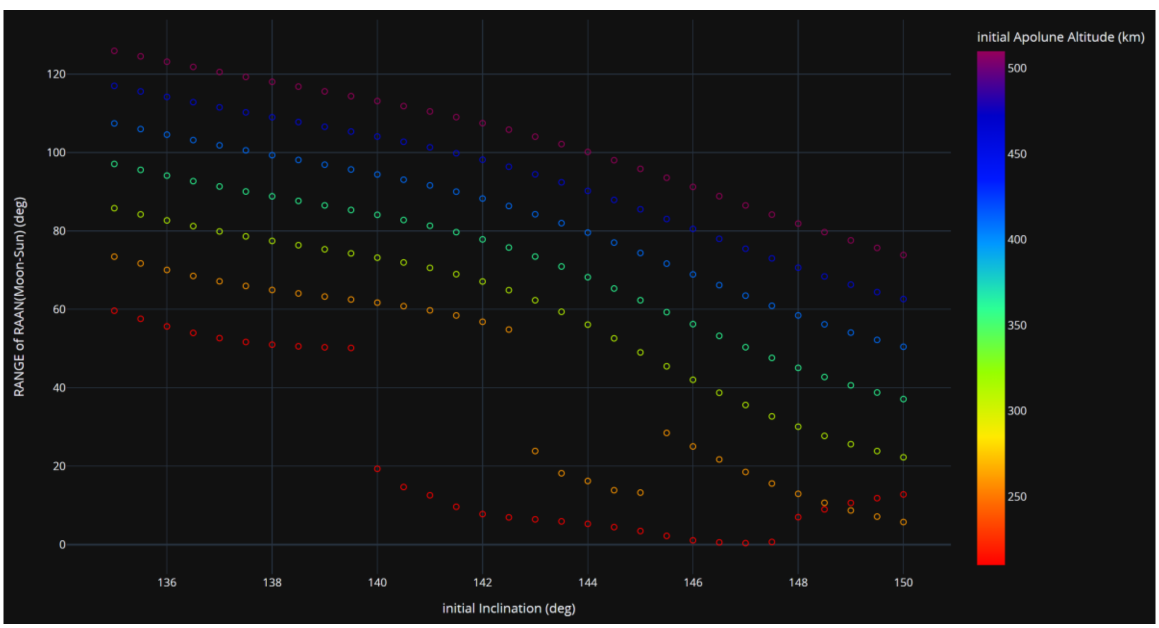

Figure 4. Numerical scan in STK fixing perilune altitude to 100 km and varying apolune.

Thus, the 100X210km orbit dimensions were fixed for the following numerical search for LSOs, which closely resembles the (N=342, M=1) case discussed in the previous section and in the companion paper [4]. The following assumptions and constraints in Table 1 were applied for this search for LSOs.

Table 1. Numerical High-Fidelity Search Assumptions & Constraints

Parameter	Assumptions & Constraints
Spacecraft	Mass = 1,000 kg, Maximum Cross-Sectional Surface Area = 5 m^2
Force Model	100X100 Moon; 30X30 Earth; 4X0 Sun; Point Masses for all other planets; Spherical Radiation Pressure
Numerical Integrator	RKF78 with Max Abs Error = 1E-13 and Maximum Relative Error = 1E-13
Initial Fixed Orbital Elements	Epoch: Jan. 4, 2027, Perilune Altitude = 100 km, Apolune Altitude = 210 km, ω = 270 deg
Propagation Duration in STK	14 days (or STOP on impact)
Design Variables (Varied parameters)	*inclination from 0.5 to 179.5 deg in 0.5 deg increments;* LAN: 0 to 360 deg. in 30-degree increments; 4,308 cases (359*12)
Primary Response Variables	Range of $RAAN_{Moon\text{-}Sun}$, Orbital Elements, & Orbit Lifetime

The numerical results of this scan are displayed in Fig. 5, where the range of $RAAN_{Moon\text{-}Sun}$ vs. initial lunar inclination is plotted with the initial LAN shown on the color bar. The lowest values of the $RAAN_{Moon\text{-}Sun}$ range reveal candidate LSOs, which result from initial lunar inclination values in the 140-170 deg range (more easily seen in Fig. 6).

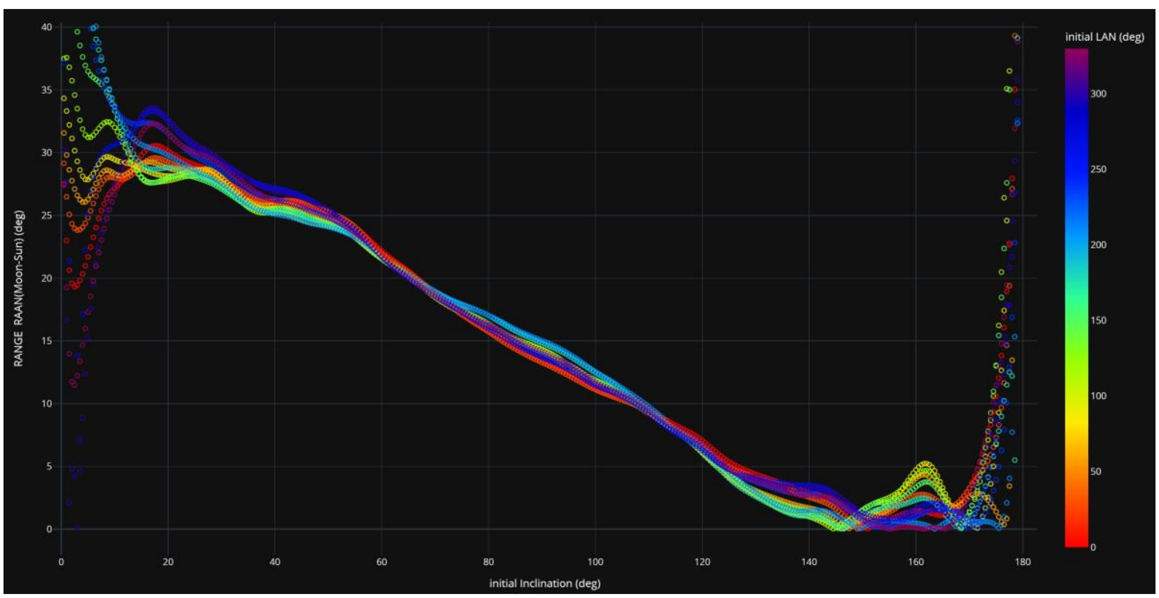

Figure 5. Full inclination scan of 100X210km low lunar orbit with 360-deg range in LAN considered to determine range of $RAAN_{Moon\text{-}Sun}$ and candidate lunar sunrise orbits.

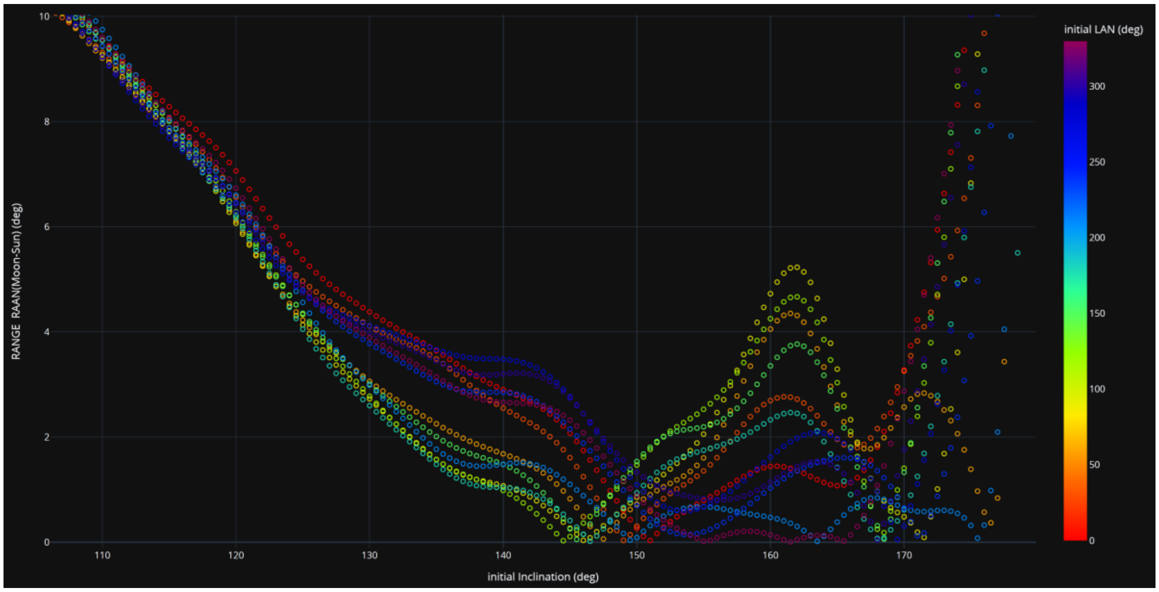

Figure 6. Full inclination scan of 100X210km low lunar orbit with 360-deg range in LAN considered to determine range of $RAAN_{Moon\text{-}Sun}$. Zoomed in near minimum values of $RAAN_{Moon\text{-}Sun}$ range to identify candidate lunar sunrise orbits.

The minimum range of $RAAN_{Moon\text{-}Sun}$ is yielded from an initial lunar inclination of 147 deg. Thus, the candidate LSO (100X210, ω=270 deg, and i=147 deg) will be applied to several CLPS missions in the sections to follow. Physically, the range of $RAAN_{Moon\text{-}Sun}$ minimized in this scan measures how far the orbit plane drifts from the Sun over the propagation, so its minimum marks the sun-synchronous inclination at which the plane holds its orientation to the Sun. The following section reaches the same candidate from the opposite direction: instead of measuring the node's swept range in a full-ephemeris propagation, it solves for the inclination whose secular nodal rate equals the solar rate in a spherical-harmonic field, recovering $i \approx 147$ deg (Figure 7).

LOW LUNAR ORBIT CORRECTION MANEUVERS FOR SUNRISE RETARGETING

When a descent from the staging LSO is waved off, the lander remains in low lunar orbit and the target site is overflown again a fixed interval later. By construction of the repeat ground track the site is re-encountered; the operational problem is to retarget that next overflight so that it occurs at local sunrise, and to do so within the lander thermal and power budget. Two figures of merit govern the recovery: the propellant cost, expressed as the maneuver ΔV, and the elapsed time of the correction, expressed as its duration. This section sizes both for the candidate LSO of the previous section (100 x 210 km, $\omega = 270°$, $i = 147°$).

All secular rates, overflight epochs, and sunrise times are evaluated in a high-fidelity force model that retains the lunar field through degree six together with the sectorial C_{22} term, a 30 x 30 Earth field, the point-mass Sun, and solar radiation pressure [5, 12]; the analytic expressions below are used to size and direct the maneuvers, and the numerical model supplies the coefficients and the final verification.

High-Fidelity Drift Through J_6 and C_{22}

The sunrise condition is set by the orientation of the orbit plane relative to the Sun, that is, by the longitude of the ascending node. Holding the node fixed in the Sun frame requires the node to precess at the selenocentric solar rate $\dot{\Omega}_{\odot} = 2\pi/T_{\oplus} \approx 0.9856°/\text{day}$. The lunar field supplies this precession through its even zonal harmonics, retained here through degree six because low-altitude lunar orbits are strongly perturbed:

$$
\begin{aligned}
\dot{\Omega} &= \dot{\Omega}_{J_2} + \dot{\Omega}_{J_4} + \dot{\Omega}_{J_6},\\
\dot{\Omega}_{J_2} &= -\frac{3}{2}\, n J_2 \left(\frac{R}{p}\right)^2 \cos i,\\
\dot{\Omega}_{J_4} &= \frac{15}{16}\, n J_4 \left(\frac{R}{p}\right)^4 \cos i\,(4 - 7\sin^2 i),\\
\dot{\Omega}_{J_6} &= -\frac{105}{128}\, n J_6 \left(\frac{R}{p}\right)^6 \cos i\,(33\sin^4 i - 36\sin^2 i + 8),
\end{aligned}
$$

where $p = a(1 - e^2)$, R is the lunar reference radius, and n is the mean motion. Solving $\dot{\Omega}(i^*) = \dot{\Omega}_{\odot}$ with the J_2 term alone gives a sun-synchronous inclination near $155°$ for this geometry; retaining J_4 and J_6 walks the solution toward the high-fidelity value. Figure 7 shows the secular nodal rate obtained by numerically propagating the 100 x 210 km geometry across inclination in the degree-six plus C_{22} field. The curve crosses the sun-synchronous rate at $i \approx 147.6°$, in close agreement with the $147°$ candidate recovered from the full-ephemeris STK scan, confirming that the candidate LSO is reproduced once the higher-degree field is included. Figure 7 is therefore the rate-based, spherical-harmonic counterpart of the full-ephemeris scan in Figures 5 and 6: the node slip on its right axis is the daily rate at which the plane departs from the Sun, and the accumulation of that rate over a propagation is precisely the $\text{RAAN}_{\text{Moon-Sun}}$ range that the STK scan minimizes, so a vanishing node slip and a vanishing $\text{RAAN}_{\text{Moon-Sun}}$ range express the same sun-synchronous condition as a rate and as a swept range. This rate view also generalizes the search: reading each CLPS site's node slip off the same curve at its limiting inclination maps directly from the single candidate found by the scan to the off-sun-synchronous application orbits whose residual drift the rest of this section corrects.

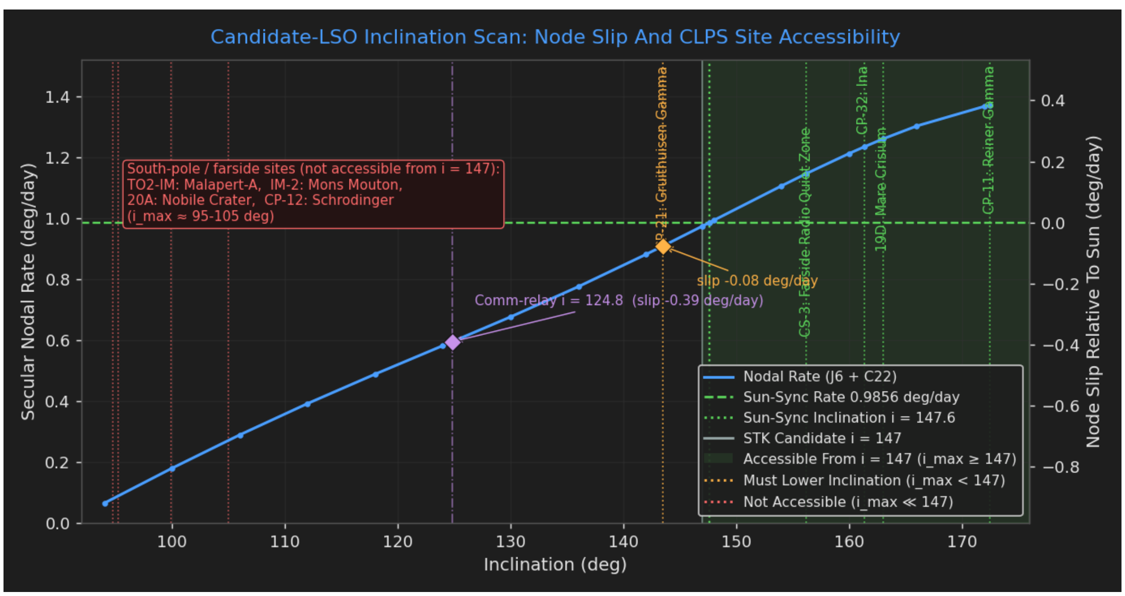

Figure 7. Candidate-LSO inclination scan: secular nodal rate versus inclination in the degree-six plus C_{22} field, node slip from the Sun on the right axis.

Reading Figure 7 this way, each CLPS site is placed on the curve at its limiting inclination i_{max} = 180 - |phi| set by its latitude, and the shaded region ($i \geq 147$ deg) marks the inclinations reachable from the selected candidate. The mid-latitude landers (Reiner Gamma, Mare Crisium, Ina, and CS-3 in the farside radio-quiet zone) are reachable at essentially zero node slip; Gruithuisen Gamma forces a lower inclination (i = 143.5 deg, slip -0.08 deg/day) and the off-sun-synchronous comm-relay orbit (i = 124.8 deg, slip -0.39 deg/day) departs further from sun-synchronicity, while the south-pole and farside sites (Malapert-A, Mons Mouton, Nobile Crater, and Schrodinger), with limiting inclinations near 95 to 105 deg, are not reachable from the selected inclination.

The sectorial term C_{22} enters differently. In an inertial frame it produces no secular nodal drift for a non-resonant orbit, but because the Moon rotates synchronously the Earth-pointing equatorial bulge is nearly fixed in the body frame, and its averaged effect is retained. Through the rotating-frame potential

$$U_{22} = \frac{\mu}{r}\left(\frac{R}{r}\right)^2 3(1 - \sin^2\varphi)(\bar{C}_{22}\cos 2\lambda + \bar{S}_{22}\sin 2\lambda),$$

where φ = selenographic latitude (measured from the Moon's equator: range of -90 to 90 degrees with positive being north and negative south) and λ = selenographic longitude (measured eastward from the Moon's prime meridian), the drift acquires a dependence on the orientation of the line of nodes relative to the Earth-Moon line, so the residual that the correction must remove depends on where in the synodic cycle the descent is missed. The companion apsidal drift, which fixes the perilune latitude and therefore the descent geometry for the $\omega = 270°$ candidate, follows the same structure, with the leading term $\dot{\omega}_{J_2} = 3/4\ n J_2 (R/p)^2 (5\cos^2 i - 1)$ and analogous J_4 and J_6 corrections. These rates are not used to design the burn directly; they size the residual drift accumulated during the correction coast, which is removed numerically.

Sunrise-Retargeting Maneuver Sequence

The lighting of any overflight is conveniently expressed as the interval after sunrise, $\tau_{\text{as}} = t_{\text{sr}} - t_{\text{fly}}$, where the sunrise epoch t_{sr} is fixed by the Sun and the true lunar orientation and the overflight epoch t_{fly} is read from the propagated ground track. An acceptable opportunity satisfies $\tau_{\text{as}} \in (0,\ 24\ \text{h}]$, the window opening at the terminator, $\tau_{\text{as}} = 0$. Because t_{sr} does not depend on the orbit, the lighting is governed one-to-one by when the spacecraft is overhead, $\partial\tau_{\text{as}}/\ \partial t_{\text{fly}} = 1$: retiming the overflight retargets the lighting by the same amount. The recovery therefore reduces to placing t_{fly} inside the fixed post-sunrise window using an in-track phasing maneuver, which adjusts arrival time without rotating the plane.

The operational sequence is as follows. After the missed descent, the staging-orbit state is propagated in the full field to predict the next overflight epoch and its τ_{as}. If the overflight already lies in the window it is taken at no propellant cost; the candidate LSO provides several such successive opportunities, spaced by one orbital period, before the site rotates out of dawn. If a correction is required, the retiming $\Delta\tau_{\text{as}}$ needed to re-enter the post-sunrise window is converted to a semi-major-axis offset over N phasing revolutions. A first tangential burn at the node nearest the approach corridor establishes the phasing orbit; the spacecraft coasts N revolutions, during which the node and apse drift at the rates above; and a second, equal and opposite burn restores the staging orbit. The corrected trajectory is re-propagated in the full field, and a small residual trim removes the drift accumulated over the coast. A period offset ΔT per revolution shifts the overflight by $\delta t_{\text{fly}} = N\,\omega_M^{-1}\Delta\lambda$ through $\Delta T = (3T/2a)\,\Delta a$, and for the two-burn sequence the total cost and elapsed time are

$$\Delta V_\phi = n\,\Delta a = \frac{2V}{3}\frac{|\Delta\tau_{\text{as}}|}{NP}, \qquad D = NP,$$

where $V \approx 1.61$ km/s and $P \approx 2.05$ hr for the candidate. The cost scales as the retiming divided by the duration: a given sunrise correction can be bought with little propellant if time is available, or quickly at higher cost. The duration is bounded above by the lead time to the targeted flyover, which for the cross-month case is the synodic interval and for the near-term case is only a few orbits. Because the staging orbit is already sun-synchronous and repeating, the maneuver nudges an overflight that already lies just outside the post-sunrise window into it rather than forcing a dawn return from an arbitrary orbit, the basis for treating the LSO as a near-zero-cost backup. The cross-month application of this sequence, recovering a missed sunrise flyover over a full lunar day of lead, is examined in the following subsection.

Ground-Track Correction Across Successive Sunrise Flyovers

The maneuver sequence above assumes the staging orbit is delivered exactly onto the candidate LSO. In practice the delivery is off-nominal: an orbit-determination or tracking error, a maneuver-execution error, or a missed descent-orbit initiation displaces the ground track or its timing, so that the first sunrise overflight of the target site is missed. Because the candidate is sun-synchronous, the next opportunity to fly over the site at local sunrise recurs one lunar day later, after a full synodic month (about 29.5 days). The operational task is therefore to apply a small in-track phasing maneuver at the missed flyover that walks the ground track back onto the site by the next sunrise overflight, using the period-biasing mechanism of the preceding subsection spread over the full month of lead time.

A single tangential phasing burn biases the orbital period, and the resulting along-track timing offset accumulates as the spacecraft completes successive revolutions, displacing the sub-satellite crossing of the site latitude in longitude in proportion to both the burn magnitude and the number of revolutions flown. Propagating the candidate in the high-fidelity field over one lunar day (approximately 345 revolutions) yields a control authority of roughly 24 km of ground-track displacement at the site per meter per second of phasing ΔV. The displacement grows linearly with the burn magnitude and the available lead time, and the numerically propagated values agree with the analytic phasing estimate to within the per-revolution libration of the crossing point, as shown in the left panel of Figure 8.

For the sun-synchronous candidate at i = 147.6 deg the orbit plane tracks the Sun, so the overflight geometry repeats from one lunar day to the next and the residual ground-track miss to be corrected is small, on the order of 15 km for the cases examined here. Phasing biases of only a few tenths of a meter per second are then sufficient: as shown in the right panel of Figure 8, biases between -0.2 and -0.8 m/s walk the next-sunrise ground track eastward across the site in steps smaller than 20 km, with a bias near -0.65 m/s placing the descending pass directly over the CS-3 site. A candidate held slightly off the sun-synchronous inclination instead accumulates an additional secular walk of approximately one degree of longitude per lunar day, which increases the required phasing bias in proportion. In every case the correction is a purely along-track adjustment of the overflight longitude; a cross-track error in the orbit node would require a small plane change and lies outside the scope of the present phasing analysis.

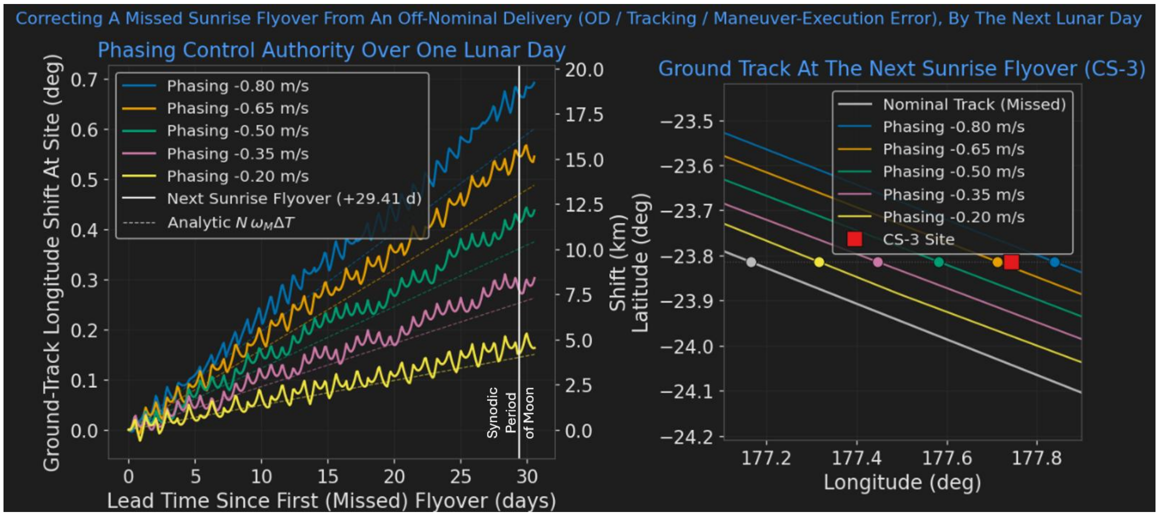

Figure 8. Correcting a missed sunrise flyover by in-track phasing (candidate i = 147.6 deg): overflight longitude shift (left) and ground tracks near CS-3 (right).

The single correction in Figure 8 is taken about one lunar day after the missed flyover. The phasing effort actually required, however, depends on how much lead time remains before the next descent attempt and on the orbit being flown, so the recovery was evaluated across a range of lead times for three representative orbits: the sun-synchronous candidate LSO (i = 147 deg, 100 x 210 km), an off-sun-synchronous circular orbit serving the same farside site (i = 124.8 deg, 108 km), and the lower-inclination orbit serving Gruithuisen Gamma (i = 142.5 deg, 100 x 210 km). In each case a nominal insertion places the first pass over the site, the descent is then missed, and a single tangential phasing burn is applied to walk a later pass back onto the site at the selected lead time. Because the candidate is already sun-synchronous, site lighting is preserved at no recurring cost; the burn corrects ground-track position only, and the reported ΔV is the one-time ground-track-positioning cost of a single establishing burn, with no restoring burn since the vehicle descends at the recovered overflight.

Each point in Figure 9 is propagator-targeted: the tangential burn is root-found so that a propagated site-latitude crossing lands on the site in the full degree-six plus C_{22} field with Earth third-body perturbations, rather than taken from a linear control-authority estimate. A correction whose semi-major-axis change exceeds the small-phasing regime ($|\Delta a|$ > 60 km) is flagged infeasible, since it is no longer a phasing maneuver. Feasible phasing recoveries (filled markers, below the small-phasing limit) occur only at the natural ground-track recurrences over the site, where they cost under 2 m/s and fall to between 0.2 and 0.67 m/s by one lunar day. At shorter lead times no phasing solution exists (crosses): closing the accumulated ground-track miss that quickly would require $|\Delta a|$ > 1000 km, that is, a non-phasing maneuver such as a plane change or a large altitude change. A missed flyover is therefore inexpensive to recover provided the next attempt is taken at the natural recurrence, but it cannot be rushed by phasing alone. The Gruithuisen case is the most constrained: with its site essentially at the orbit's turning latitude, it recovers only at one lunar day, the sensitivity that motivates carrying a small inclination margin rather than placing a site exactly at the maximum reachable latitude.

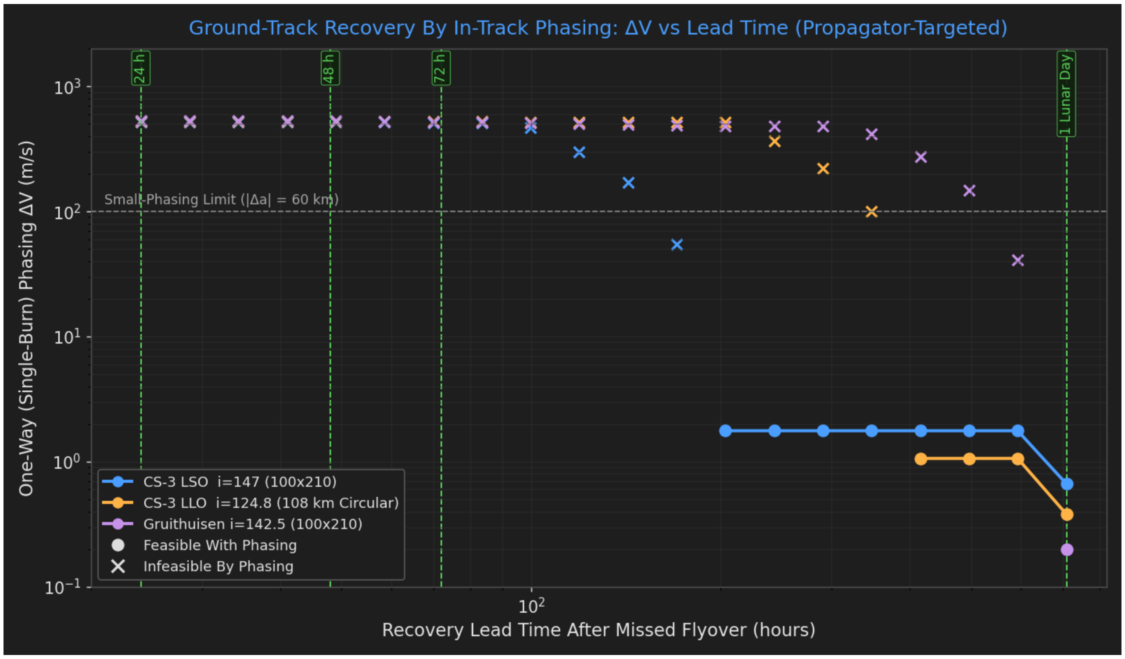

Figure 9. Ground-track recovery from a missed flyover by in-track phasing for three orbits: single-burn phasing ΔV versus available lead time.

Applications to CLPS Missions

Having established the sunrise-retargeting and ground-track recovery maneuvers above, this subsection applies them to specific CLPS missions. Below in Table 2 is a list of CLPS missions, both past and planned. The landing status of each mission is stated along with the landing region and/or approximate site coordinates. The following discussion applies LSOs to CLPS missions with mid-latitude landing sites.

The candidate LSO specified in the previous section: **100X210, *ω*=270 deg, and *i*=147 deg** is directly applicable to many CLPS missions listed above with mid-latitude landing sites such as Mare Crisium (+17, +59.1), Reiner Gamma (+7.5, -59), and CS-3 (-20, 180). However, the CLPS CP-21 mission plans for a landing site among the Gruithuisen Dome (+36.5, -40.8), thus the initial lunar inclination will be decreased from 147 to 143.5 deg to ensure access to the surface from LLO without a significant plane-change maneuver. NASA's *Lunar Browser* [11, 13] tool is used for Earth-Moon transfer trajectory selection via filtering from a set of ~500,000 trajectories from Earth launch and trans-lunar injection to lunar orbit insertion.

The inclination that makes the candidate orbit sun-synchronous also fixes the band of latitudes it can serve: a retrograde LSO reaches a maximum latitude of 180 deg minus its inclination, so the i = 147 deg candidate accesses sites within about 33 deg of the equator. As shown in Figure 7, the mid-latitude CLPS sites of Table 2 — Reiner Gamma (+7.5 deg), Mare Crisium (+17 deg), Ina (+18.7 deg), and the radio quiet zone on the lunar farside (-23.8 deg) — all have limiting inclinations above the sun-synchronous value, so each is reached by the sun-synchronous orbit itself at essentially zero node slip, with no secular sunrise drift to fight.

Table 2. CLPS Mission Lunar Landing Sites & Status

Number	Name	Contractor	Launch Vehicle	Lander	Landing Region	Landing Site (Lat., Long.), deg.	Mission Status
TO2-AB	Peregrine Mission One	Astrobotic Technology	Vulcan Centaur VC2S	Peregrine	Nearside: Mons Gruithuisen Gamma	(+36.46, -40.8)	DID NOT LAND (Launched: Jan. 8, 2024)
TO2-IM	IM-1	Intuitive Machines	Falcon 9 Block 5	Nova-C Odysseus	South Pole: Malapert-A	(-80.13, 1.44)	LANDED (Feb. 22, 2024)
19D	Blue Ghost Mission 1	Firefly Aerospace	Falcon 9 Block 5	Blue Ghost	Nearside: Mare Crisium	(+17, +59.1)	LANDED (March 2, 2025)
CLPS-3	IM-2	Intuitive Machines	Falcon 9 Block 5	Nova-C Athena	South Pole: Mons Mouton	(-84.8, 29.1)	LANDED (March 6, 2025)
CT-3	Blue Moon Pathfinder 1	Blue Origin	New Glenn	Blue Moon Mark 1	South Pole	TBA	PLANNED (NET 2026 Q1)
CP-11	IM-3	Intuitive Machines	Falcon 9 Block 5	Nova-C	Nearside: Reiner Gamma	(+7.5, -59)	PLANNED (NET 2026)
CS-3	Blue Ghost Mission 2	Firefly Aerospace	TBA	Blue Ghost	Farside: Radio Quiet Zone	(-23.8, -177.7)	PLANNED (NET 2027)
20A	Griffin Mission I	Astrobotic Technology	Falcon Heavy	Griffin	South Pole: Nobile Crater	(-85.28, 53.27)	PLANNED (NET July 2026)
CP-12	*ispace* Mission 3	Draper Laboratory	TBA	APEX 1.0	Farside: Schrodinger Basin	(-75, 132.4)	PLANNED (NET 2027)
CP-22	IM-4	Intuitive Machines	TBA	Nova-C	South Pole: Mons Mouton	(-84.6, 31)	PLANNED (NET 2027)
CS-7	Blue Moon Pathfinder 2	TO CS-7	New Glenn	Blue Moon Mark 1	South Pole	TBA	PLANNED (late 2027)
CP-21	Blue Ghost Mission 3	Firefly Aerospace	TBA	Blue Ghost	Nearside: Mons Gruithuisen Gamma	(+36.46, -40.8)	PLANNED (NET 2028)
CT-4	TBA	TBA	TBA	TBA	South Pole	TBA	PLANNED (TBD)
Moon Base: CS-8	TBA	Astrobotic, Firefly, & Intuitive Machines	TBA	TBA	TBA	TBA	PLANNED NET 2028
CP-32	TBA	TBA	TBA	TBA	Ina Volcanic Crater	(+18.66, 5.3)	PLANNED (TBD)
CS-6	TBA	TBA	TBA	TBA	South Pole	TBA	PLANNED (TBD)

For these sites a missed sunrise descent is recovered at the next lunar dawn by the small in-track phasing analyzed above, of order a few tenths of a meter per second; the -0.65 m/s that recentered the CS-3 ground track in Figure 8 is representative. The lighting tolerance is generous, so the binding requirement for these recoveries is placing the ground track back over the site rather than the sunrise timing itself. The Gruithuisen Dome site of CP-21 (+36.5 deg latitude) forces the inclination down to: (180 - 36.5) deg = 143.5 deg, just below the crossing, where the node slips only about -0.08 deg/day relative to the Sun; this remains nearly sun-synchronous, and the sunrise geometry is held with a small per-month phasing maneuver. The CS-3 comm-relay scenario, which holds the inclination near 124.8 deg for coverage reasons, slips about -0.39 deg/day and lies furthest from the sun-synchronous condition, carrying the largest station-keeping budget of the cases considered, with the cost scaling with that slip through the phasing relation given above.

CLPS CS-3 Mission: Farside: approx. (-23.8, 177.7)

The CS-3 mission is relatively complex given the planned deployment of a communications relay satellite in elliptical frozen orbit before the descent to LLO and the lunar surface. Thus, two scenarios are applied to this mission application: one with a 147-degree low-altitude LSO (with deployment of the communications relay satellite in a lunar elliptical orbit with the same inclination) and the other with a nominal inclination of ~124.8 degrees for both the relay orbit and LLO.

In the first scenario, a 750 km perilune altitude is targeted for the communications relay satellite with inclination of 147 degrees to ensure the LLO is a LSO. This low-altitude LSO has a lifetime of 84 days without station-keeping maneuvers and enables up to 3 landing attempts at lunar dawn at the selected site on the lunar farside (Figs. 10 & 11).

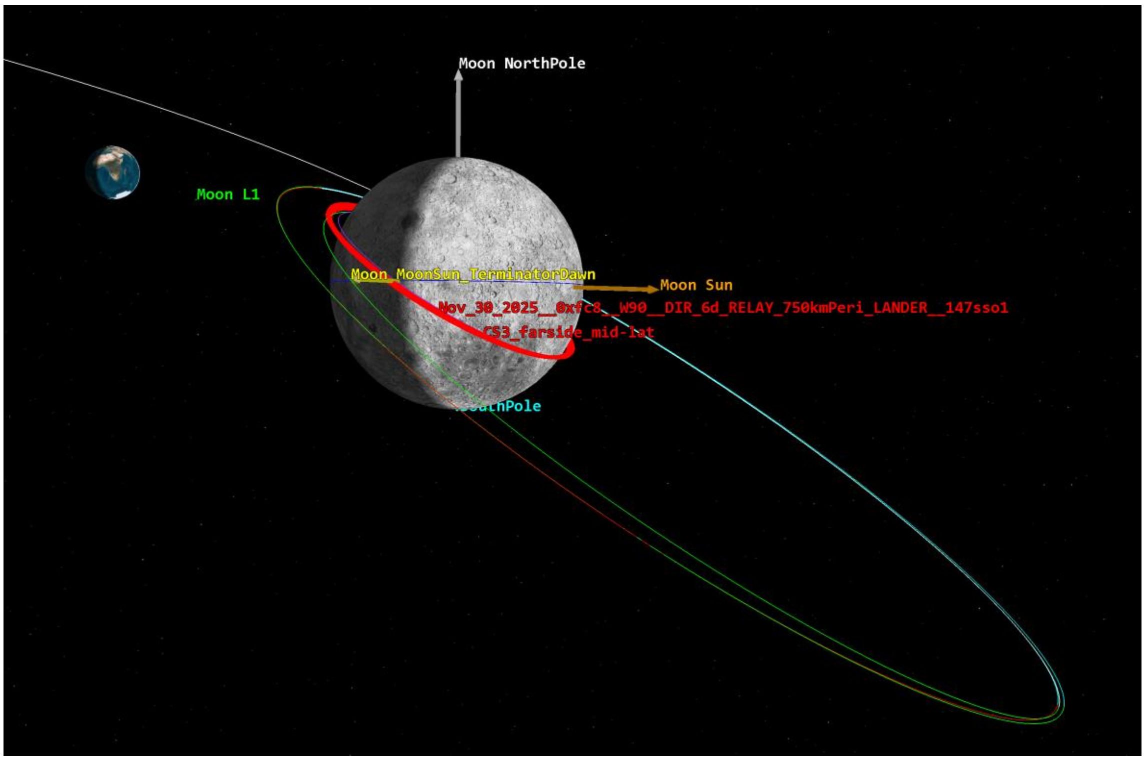

Figure 10. CS-3 application: communications relay satellite dropped off elliptical lunar orbit with 750 km perilune altitude, while LSO inclination = 147 degrees with orbit lifetime of 84 days. Viewed in Moon-Sun rotating frame.

The second scenario uses what may still be referred to as an LSO as this orbit does yield flyovers of the landing site at successive sunrises by allowing the LAN to rotate 360-degrees every lunar dawn (Fig. 12). However, this orbit's ground track is not fixed over the landing site every orbit like a true RGT orbit. This LAN rotation is done by first iterating on the LLO altitude and if needed, iterating on the inclination.

With iteration on only the LLO altitude from 100 km to 108 km it is found that near-repeating ground tracks are yielded which allows for backup dawn landing windows while also maintaining the frozen inclination of the comm relay orbit, thus minimally changing the nominal mission while increasing mission resiliency.

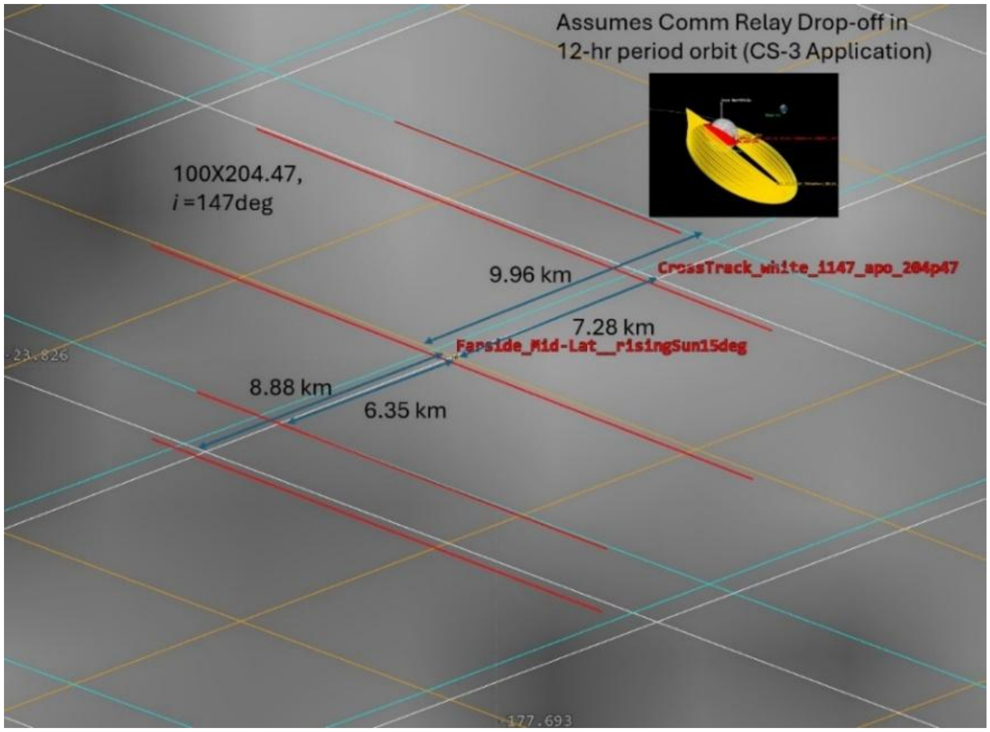

Figure 11. Lunar sunrise orbit shows its ground track is nearly dawn-repeating. Assumes communications-relay satellite drop-off in elliptical lunar orbit with same inclination (147 deg) as lunar sunrise orbit.

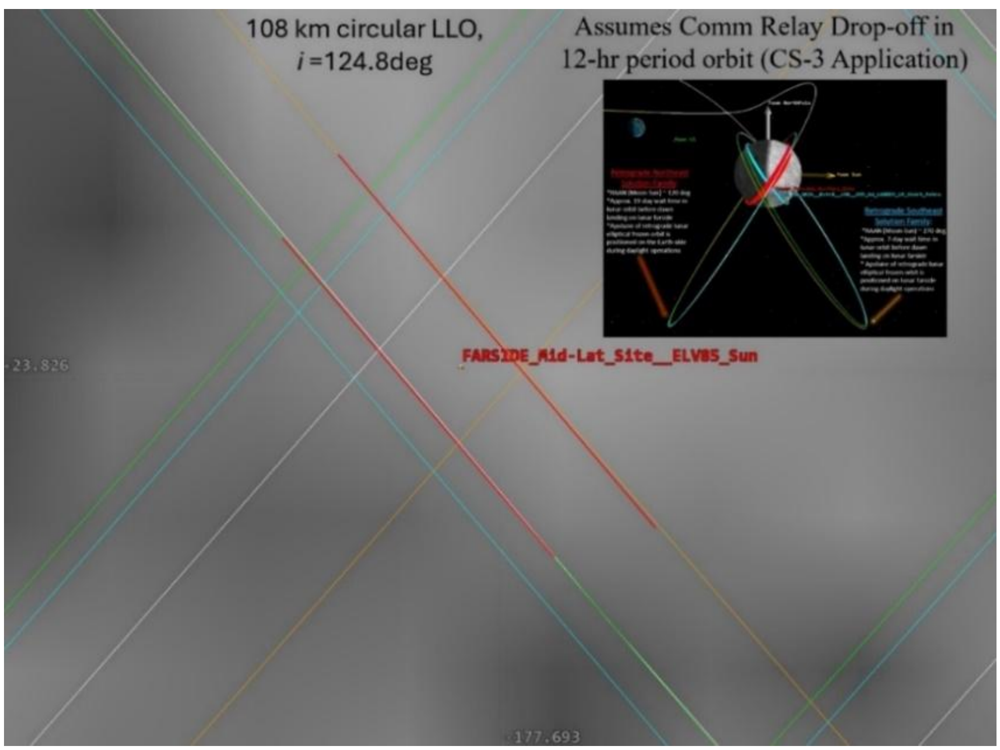

Figure 12. Lunar dawn-repeating ground track with LAN rotation throughout lunar day. Assumes communications relay satellite drop-off in elliptical lunar frozen orbit.

SUMMARY

Methods for computing lunar sunrise orbits (LSOs) were presented, with results from numerical scans in STK Astrogator that agree with the companion paper [4]. The scan identified a representative candidate LSO, a 100 x 210 km orbit with $\omega = 270$ deg and $i = 147$ deg, that is sun-synchronous with a repeating ground track and is directly applicable to CLPS missions with mid-latitude landing sites (e.g., Mare Crisium, Reiner Gamma, and the farside radio-quiet zone).

Low-lunar-orbit correction maneuvers for sunrise retargeting were then developed to make this candidate a resilient staging orbit. When a descent is waved off, the lander remains in low lunar orbit and the repeat ground track re-encounters the site a fixed interval later; the recovery problem is to retarget that next overflight so it falls within the post-sunrise lighting window, inside the lander thermal and power budget, and is governed by two figures of merit: the maneuver ΔV and the correction duration. All secular rates, overflight epochs, and sunrise times were evaluated in a high-fidelity force model (the lunar field through degree six with the sectoral C_{22} term, a 30 x 30 Earth field, the point-mass Sun, and solar radiation pressure). Because the sunrise condition is fixed by the orbit-plane orientation relative to the Sun, sun-synchronicity requires the node to precess at the solar rate; the even zonal harmonics supply this precession, and a numerical nodal-rate scan (Figure 7) crosses the sun-synchronous rate near $i = 147.6$ deg, reproducing the full-ephemeris STK candidate once the higher-degree field is included.

Since the lighting depends one-to-one on when the spacecraft is overhead, the recovery reduces to an in-track phasing maneuver that adjusts arrival time without rotating the plane, and two recovery regimes were sized. In the near-term regime, the sun-synchronous repeat track provides several successive dawn overflights spaced by one orbital period, so a missed descent is frequently recovered at a later pass at no additional propellant cost, or with a small phasing correction of only a few orbits' duration; the two-burn establish-and-restore sequence costs a ΔV that scales as the required retiming divided by the available duration, so it can be bought cheaply when lead time is available. In the cross-month regime, an off-nominal delivery (an orbit-determination, tracking, or maneuver-execution error, or a missed descent-orbit initiation) causes the first sunrise overflight to be missed, and because the orbit is sun-synchronous the next sunrise opportunity recurs one lunar day (one synodic month, about 29.5 days) later. A single in-track phasing burn then walks the ground track back onto the site over that interval; the candidate provides a control authority of about 24 km of ground-track displacement per m/s of phasing ΔV over the roughly 345 revolutions of a lunar day, and since sun-synchronicity keeps the residual miss small (~15 km), biases of only a few tenths of a m/s suffice, with a bias near -0.65 m/s recentering the descending pass on the CS-3 site (Fig. 8).

The single-burn recovery cost was then characterized against the available lead time for three representative orbits using a propagator-targeted differential corrector (Figure 9). Feasible phasing recovery, one that stays within the small-phasing regime ($|\Delta a| \leq 60$ km), is confined to the natural ground-track recurrences over the site, where it costs under 2 m/s and falls to between 0.2 and 0.67 m/s by one lunar day; at shorter lead times no phasing solution exists, since closing the accumulated miss that quickly would demand $|\Delta a| > 1000$ km, i.e. a non-phasing maneuver. Because the staging orbit is already sun-synchronous and repeating, the recovery nudges an overflight that already lies near the dawn window rather than forcing a dawn return from an arbitrary orbit, the basis for treating the LSO as a near-zero-cost backup that adds landing-opportunity resilience for these CLPS missions. The most constrained case is the Gruithuisen-serving orbit, whose site sits essentially at the orbit's turning latitude and recovers only at one lunar day; this sensitivity motivates carrying a small inclination margin (here the candidate inclination was lowered from 147 to 143.5 deg for the CP-21 mission at ~36.5 deg latitude) rather than placing a site exactly at the maximum reachable latitude.

REFERENCES

[1] Bussey, B. et al. (2019) *AGU Fall Meeting*. PA54B-11.

[2] National Aeronautics and Space Administration, “Commercial Lunar Payload Services,” https://www.nasa.gov/commercial-lunar-payload-services/, 2025, Accessed: 2026-02-15.

[3] Russell, R. P. and Lara, M., “Long-Lifetime Lunar Repeat Ground Track Orbits,” Journal of Guidance, Control, and Dynamics, Vol. 30, No. 4, 2007, pp. 982–993.

[4] Van Hammond, C. J., Russell, R. P., and Genova, A. L., “Sun-Synchronous Orbits at the Moon,” AAS/AIAA Astrodynamics Specialist Conference, Boston, MA, 2026, AAS Paper 26-XXX.

[5] Konopliv, A. S., Park, R. S., Yuan, D. N., et al., “The JPL lunar gravity field to spherical harmonic degree 660 from the GRAIL Primary Mission,” Journal of Geophysical Research: Planets, Vol. 118, No. 8, 2013, pp. 1415–1434, High-resolution lunar gravity field from GRAIL data.

[6] Pines, S., “Uniform Representation of the Gravitational Potential and its Derivatives,” *AIAA Journal*, Vol. 11, No. 11, 1973, pp. 1508–1511.

[7] Szebehely, V., “Description of the Restricted Problem,” Theory of Orbits: The Restricted Problem of Three Bodies, chap. 1, Academic Press, New York, 1967, See especially Sec. 1.4, “Equations of Motion in a Synodic Coordinate System and the Jacobian Integral”.

[8] McArdle, S. and Russell, R. P., “Stable Low Altitude Lunar Periodic Orbits Using the GRAIL Gravity Field,” AAS/AIAA Astrodynamics Specialist Conference, 2019.

[9] Lara, M., “On the frozen orbits of a satellite,” Celestial Mechanics and Dynamical Astronomy, Vol. 101, 2008, pp. 389–399.

[10] McArdle, S. and Russell, R. P., “Circulating, Eccentric Periodic Orbits at the Moon,” Celestial Mechanics and Dynamical Astronomy, 2021.

[11] Genova, A. L., Morrison-Fogel, D., & Levinson-Muth, P., “Transfers from TLI to Lunar Frozen Orbits with Applications to NASA’s CLPS & Artemis Programs,” AAS/AIAA Space Flight Mech. Mtg., Orlando, FL, Jan. 8-12, 2024.

[12] Zuber, M. T., Smith, D. E., Watkins, M. M., & Binder, A. B., “Gravity Field of the Moon from the Gravity Recovery and Interior Laboratory (GRAIL) Mission,” Science, 2013.

[13] Genova, A. L., Morrison-Fogel, D., Levinson-Muth, P., Dono Perez, A., & Blue, R., “Lunar Browser trajectory tool,” Software for the NASA Science Mission Directorate Workshop,” Washington, DC, May 7-9, 2024.

[14] Vallado, D. A., Fundamentals of Astrodynamics and Applications, 4th ed., Microcosm Press, Hawthorne, CA, 2013, Chap. 6.